Effectiveness study of wire mesh vibration damper for sensitive equipment protection from seismic events

Fares MEZGHANI, Alfonso Fernández DEL RINCÓN*, Pablo García FERNANDEZ, Ana de-Juan, Javier Sanchez-Espiga, Fernando Viadero RUEDA

Laboratory of Structural and Mechanical Engineering, Superior Technical School of Industrial Engineering and Telecommunications, University of Cantabria, Santander, Spain

Abstract

Wire Mesh Vibration Damper (WMVD) is proposed for the protection of vibration-sensitive equipment, such as Information Technology (IT) equipment, from seismic events. The mathematical model of the proposed isolator is primarily defined and then implemented to develop the Matlab Simscape Multibody^{TM} model of the WMVD isolated system subjected to earthquake induced floor motion. The latter is simultaneously generated for natural earthquake records and scaled to satisfy the GR-63-CORE (Zone 4) standard requirements via an artificial seismic time-history generation procedure, developed in the present work. In order to study the isolation effectiveness of the WMVD, comparative analysis with linear anti-seismic support is firstly provided. Results reveal that the WMVD isolated system can effectively attenuate seismic response more than 85 % , whereas the seismic responses of the linearly isolated system increase by 160 % as compared to the ground motion acceleration. Subsequently, an Incremental Dynamic Analysis (IDA) by specifying the operational vibration limit of the sensitive equipment mounted on the WMVD, is conducted to create the fragility curves. Considering the maximum acceleration response as engineering demand parameter, seismic fragility analysis eventually demonstrates the performance of the WMVD to protect the sensitive equipment from floor motion excitation.

Keywords: Wire Mesh Vibration Damper, Vibration-sensitive equipment

*Corresponding author. E-mail address: fernandra@unican.es

protection, Matlab Simscape Multibody^{TM} model, Artificial seismic time-history generation procedure, Comparative analysis, Fragility analysis.

1. Introduction

Earthquake, an intense trembling of Earth's surface, leads not only to injury and loss of human life, but also to significant economic losses because of resulting in huge destruction of rigid structures and collapse or destabilization of buildings. In recent years, the world encountered catastrophic outcomes where structures and buildings are not well-protected against high magnitude and long period seismic events. Therefore, finding effective seismic protection techniques has become one of the top priorities for the engineering community.

Seismic isolation technology has been extensively used to protect structures and non-structural components from ground and floor motions induced by earthquakes. Nowadays, several seismic isolation strategies have been provided to reduce the damaging effects on components ranging from civil buildings [1–5] and bridges [6–8], to industrial structures [9, 10], to floors within a building [11–13]. Equally important is the application of seismic isolation technology in the sensitive equipment inside a building such as Information Technology (IT) equipment (e.g., computer servers, mainframes, LAN racks). In many cases, the monetary loss due to damage of IT equipment housed in buildings substantially exceeds the value of damage to the main structure itself [14]. In general, there are three ways to successfully retain the performance of sensitive equipment using seismic isolation concept, implemented at various scales [15]: (1) the entire housing structure, (2) floors inside the structure and (3) the interior component level. The third approach has the potential of offering the best of the first approach with lower cost and overcoming the second approach difficulty related with ensuring enough vertical stiffness to support the equipment itself [16].

In the literature, passive and semi-active isolation systems have been widely applied to reduce the transmitted vibration energy by mechanically decoupling the motion of the equipment and their contents from the building floor motion [17, 18]. Several passive equipment isolation systems have been developed and utilized on non-structural systems and equipment that can be particularly fragile to seismic effects. Typically, two configurations of isolation systems are considered; friction-type [19] and rolling-type [20] systems.

List of Abbreviations

CRS	Calculated Response Spectrum
EDP	Engineering Demand Parameter
GRS	Given Response Spectrum
$HWRI$	Helical Wire-Rope Isolator
IDA	Incremental Dynamic Analysis
IM	Intensity Measure
IT	Information Technology
MAR	Maximum Acceleration Responses
PGA	Peak Ground Acceleration
$PSDMs$	Probabilistic Seismic Demand Models
$RISs$	Rolling Isolation Systems
RRS	Required Response Spectrum
SCF	Sliding Concave Foundation
$SDI–BPS$	Static Dynamic Interchangeable-Ball Pendulum System
$WMVD$	Wire Mesh Vibration Damper
WRI	Wire-Rope Isolator
ZPA	Zero Period Acceleration

An effective way, to protect the interior vulnerable equipment of buildings, consists in incorporating a Sliding Concave Foundation (SCF) system [14] into a raised floor system. The performance of the isolation system was evaluated in terms of its response and different real earthquakes were employed. Harvey and Gavin [21] modeled and tested a novel double Rolling Isolation Systems (RISs) that consists of two individual Rolling Isolation Systems stacked one on top of other. The mathematical model and experimental validation were carried out to analyze the performance of double (RISs) that possesses greater displacement capacity than that of its constituent subsystems alone.

The friction-type or rolling-type seismic isolators are systems provided natural periods of 2 sec to 4 sec [22]. The excessive displacement response of the long period isolation systems could damage the isolators even the equipment during high-amplitude and long period ground motions [23]. Moreover, the friction-pendulum or rolling-pendulum isolation systems are not enough to effectively reduce the vibration response of lightweight equipment. To reach the desired isolation range, low-mass isolated structure should be connected to low-stiffness isolation system [24]. Otherwise, these systems implement ball with relatively fixed geometry, thus the isolators will be not suitable to mitigate transmitted excitation for a wide range of structure and ground motion characteristics [25].

To prevent this situation, Gavin and Zaicenco [22] proposed the use of semi-active isolation system in order to protect light equipment within buildings, subjected to different unidirectional ground motions. The results illustrated the improvements associated with semi-active equipment isolator comparing to passive equipment isolation systems in terms of the peak response accelerations reduction. Lu et al. [26] suggested the use of fuzzy-controlled semi-active isolation system as effective technology to alleviate the excessive seismic response when isolated system is subjected to near-fault earthquakes, containing strong long-period wave components. However, semi-active systems are more complicated (i.e. content sensors and actuators), thus, may require more maintenance than passive isolation systems [27].

Recent studies investigated the isolation performance of metallic dampers that dissipate energy through the inelastic deformation of constitutive substances. Javanmardi et al. [28] provided a review of recent development and applications of metallic dampers in vibration control systems. This article revealed the advantages of metallic dampers over semi-active isolators due to their stability of the hysteretic behavior, low cost, resistance to temperature variation and high energy dissipation capability. It is also concluded that amongst several passive isolators types, the metallic dampers have gained attention for their ability to protect equipment from seismic events caused damage. Paolacci and Giannini [29] proposed a steel cable damper (Wire-Rope Isolator (WRI)) as seismic isolator to reduce the vulnerability effect on the electrical equipment. Massa et al. [30] adopted, in parallel with the WRI, a ball bearing that provides additional vertical stiffness to support the normal load of the sensitive equipment and low horizontal stiffness to allow the lateral movement of the equipment with low friction. Alessandri et al. [31] demonstrated the effectiveness of Helical WRI (HWRI) in reducing seismic response of electrical systems due to the mechanical flexibility and friction between wires that provide optimal isolation properties.

While research on seismic control systems is developing, metallic dampers may be still improvable to offer higher performance to protect sensitive equipment under moderately strong or strong earthquake. In this paper, a promising Wire Mesh Vibration Damper (WMVD), related to the combination of a knitted stainless steel wire cushion with a coil spring, is presented as seismic mitigation solution to protect vibration-sensitive equipment. This type of wire mesh damper can give not only high damping rate due to the contacts between adjacent wires [32] but also good vibration control capacity within low frequency range. Because of these attractive properties, WMVD can be adopted as one of the most economical and effective mechanisms available for the input energy dissipation during an earthquake with long-period components. The purpose of this study is to assess the effectiveness of the WMVD designed for protecting IT equipment from earthquake motion. As a first focus, this paper is addressed to determine the dynamic seismic response of the equipment mounted on the WMVD through time-history analysis. To deal with this aim, the mathematical model of the proposed isolator is primarily defined and then implemented to develop the Matlab Simscape Multibody^{TM} model of the WMVD isolated system subjected to earthquake induced floor motion. The multibody model is automatically generated by the Simscape Multibody^{TM} solver and thus the response of the system is simulated without need to dynamic equations. The second focus of this paper, to reliably assess the performance of the proposed seismic isolator, is on the fragility analysis, which requires sets of accelerograms describing the natural variability of the building floor motions.

The paper is organized as follows. Firstly, the multibody model of the WMVD isolated system and an efficient procedure for the generation of artificial accelerograms are presented in Section 2. Section 3 utilizes the developed model and the artificial accelerogram generation procedure for the time-history analysis of the WMVD isolated system. According to the incremental dynamic analysis results, Section 4 evaluates the performance of the WMVD using seismic fragility analysis. Finally, the conclusions of the study are summarized in the last section.

2. Wire mesh vibration dampers isolated system

In this study, the sensitive equipment is assumed to be a rigid body and considered as a single-degree-of-freedom (SDOF) system connected to the base through the anti-seismic support with metallic dampers. As shown in Figure 1, the WMVD isolated system is excited by a single vertical component of the base acceleration, thus only the acceleration responses in the vertical direction are examined. Furthermore, the damper mass is considered negligible with respect to the system mass, and the assumption remains valid regardless of the isolated equipment mass. This is mainly because the studied damper is desired to isolate the IT equipment with relatively high weight. Therefore, the isolator is massless [33] and is modeled as spring-damper with variable stiffness and damping, depending on the displacement and velocity.

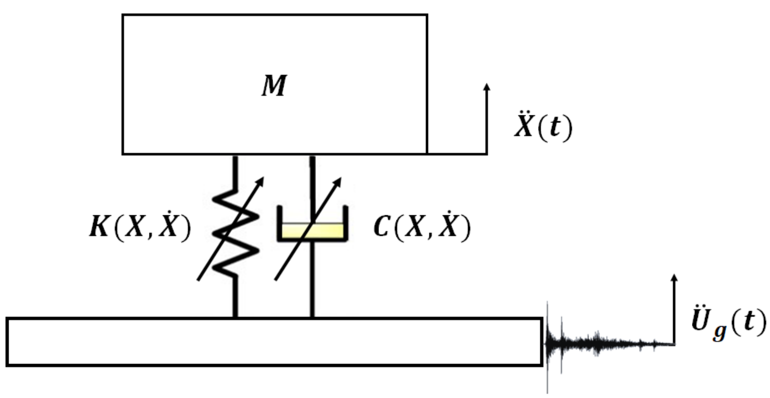

Figure 1. Single-degree-of-freedom model of WMVD isolated system

The WMVD isolated system (see Figure 2(a)) is attached to the n^{th} floor of the primary structure (building), when a seismic event is significantly amplified and the floor motion definitely contains strong long-period wave components. Figure 2(b) illustrates the commercial anti-seismic support, which is composed of five WMVD vertically placed between the upper and lower plates fixed to the isolated object and the floor, respectively. The dimensions ($H \times D \times W$) of the studied anti-seismic support are 80 mm $\times$

$130\,mm \times 180\,mm$ and dampers spacing are taken to be $l_x = 60\,mm$ and $l_y = 70\,mm$, as shown in Figure 2(c). Each WMVD (Figure 2(d)) is given as a combination of linear coil-spring and nonlinear metallic cushion damper, which is mainly made up of a stainless steel wires, woven, rolled and pressed into a cylindrical geometric shape.

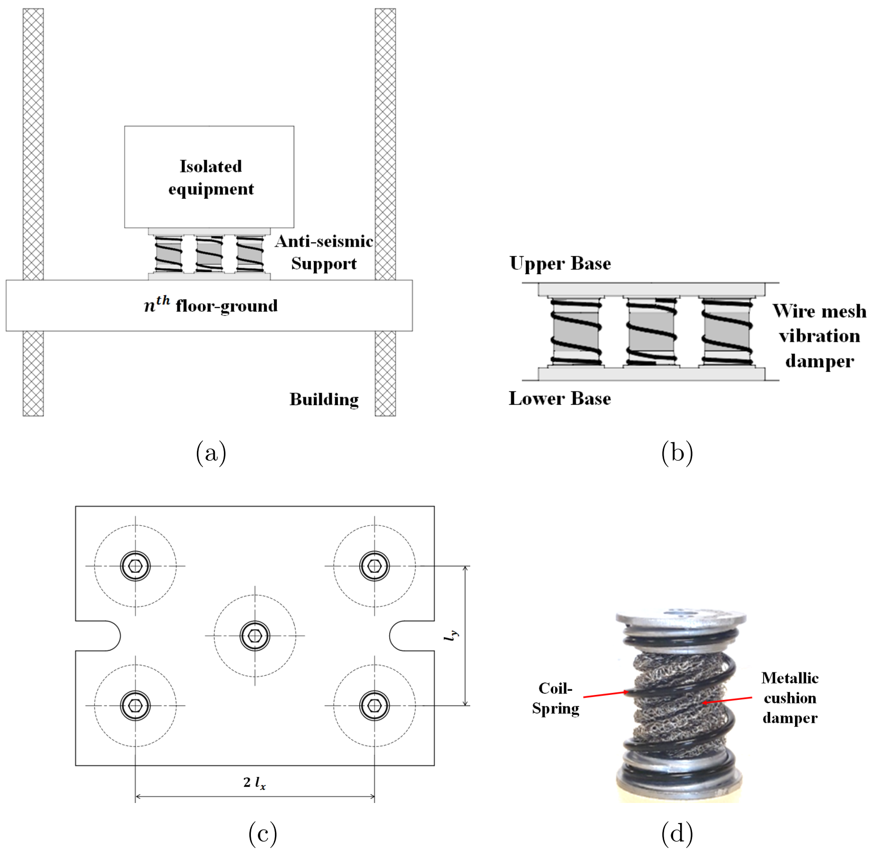

Figure 2. (a) WMVD isolated system attached to the n^{th} floor-ground, (b) The commercial anti-seismic support, (c) Plan dimension of the anti-seismic support and (c) Wire mesh vibration damper

In this section, the modeling of the individual WMVD as well as the validity of the mathematical model are first discussed. Secondary, the defined model is implemented in the Multi-body model of the WMVD isolated system to predict the seismic response. The system is subjected to the earthquake induced floor motion that is then simulated via artificial generation procedure.

2.1. Identification and validation of the individual WMVD model

Before modeling the whole isolation system, the individual WMVD is evaluated firstly in terms of its stiffness and damping characteristics. The stiffness/damping model is obtained by means of a nonparametric identification method, previously proposed and experimentally validated [34]. To guarantee that the identified properties of the WMVD are consistent with the seismic simulation, presented in Section 3, the resonance research test is conducted according to the Standard Test Procedure for the Seismic Qualification [35]. The experiment is carried out by sweeping the frequency excitation of the system in the vertical direction and keeping the acceleration level constant in $2\,m/s^2$ ($\sim 0.2\,g$). Two uni-axial accelerometers are rigidly placed on the shaker table and on the isolated mass to record the vertical components of the acceleration responses. For the individual WMVD modeling, the nonlinear identification is concentrated only in the first resonance related to the vertical direction.

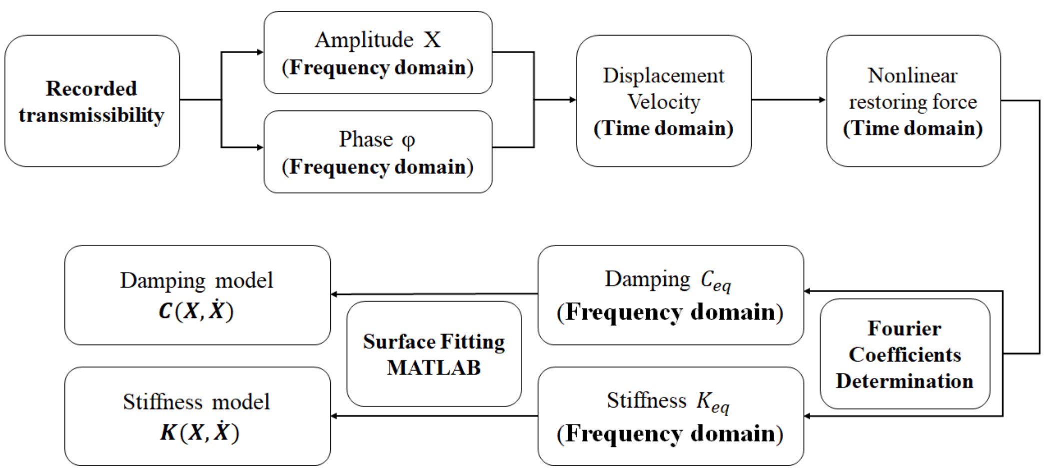

Figure 3. Flow chart of the nonparametric identification method

Based on the mathematical model shown in Figure 1, The dynamic equation of the WMVD isolated system is written as:

$$M\,\ddot{X}(t) + C(X,\dot{X})\,\dot{X}(t) + K(X,\dot{X})\,X(t) = -M\,\ddot{U}_g(t) \tag{1}$$

where M is the mass and $\ddot{U}_g$ denotes the ground excitation. X presents the relative displacement between the isolated mass and the base, which is the deformation of the mount (including the static deflection). $K(X,\dot{X})$ and

$C(X, \dot{X})$ correspond respectively to the nonlinear stiffness and damping that depend on the displacement and velocity response amplitudes.

An extension of the existing identification method is performed to develop the mathematical model, related the displacement and velocity with nonlinear stiffness and damping. As shown in the flow chart of the nonparametric identification method (Figure 3), the response amplitude and phase, in the frequency domain, are computed from the recorded transmissibility. Expressing the displacement $X(t)$ and the velocity $\dot{X}(t)$ in truncated Fourier series, the nonlinear restoring force can be determined using Eq.(1). Once the equivalent stiffness and damping are obtained, the stiffness and damping models (Eq.(2) and Eq.(3), respectively) can be defined throughout the least squares polynomial approximation, via surface fitting Matlab toolbox. It should be mentioned that the present model is valid for the displacement and velocity ranges corresponding to the excitation level. The maximum amplitudes of displacement and velocity are within the ranges of $0.5\ 10^{-3} - 7\ 10^{-3}$ m and $0.05 - 0.3\ m/s^2$, respectively.

$$K(X, \dot{X}) = \sum_{i=0}^{N_1} \sum_{j=0}^{N_2} P_{ij}^{stiff} B_{ij}^{stiff}(X, \dot{X}) \tag{2}$$

$$C(X, \dot{X}) = \sum_{i=0}^{N_1} \sum_{j=0}^{N_2} P_{ij}^{damp} B_{ij}^{damp}(X, \dot{X}) \tag{3}$$

where P_{ij}^{stiff} and P_{ij}^{damp} are unknown coefficients for stiffness and damping polynomial functions, respectively. N_1 and N_2 present the polynomial order and $B_{ij}^{stiff}(X, \dot{X})$ and $B_{ij}^{damp}(X, \dot{X})$ correspond to the basic functions, which are power expansion of X and $\dot{X}$. The basic function of the stiffness (Eq.(4)) is obtained by substituting $N_1 = 5$, $N_2 = 0$, however, the damping basic function (Eq.(5)) is obtained by choosing $N_1 = 3$, $N_2 = 2$.

$$B_{ij}^{Stiff}(X) = \left\{1, X, X^2, X^3, X^4, X^5\right\} \tag{4}$$

$$B_{ij}^{Damp}(X, \dot{X}) = \left\{1, X, X^2, X^3, \dot{X}, \dot{X}^2, \dot{X}X, \dot{X}^2X, \dot{X}X^2\right\} \tag{5}$$

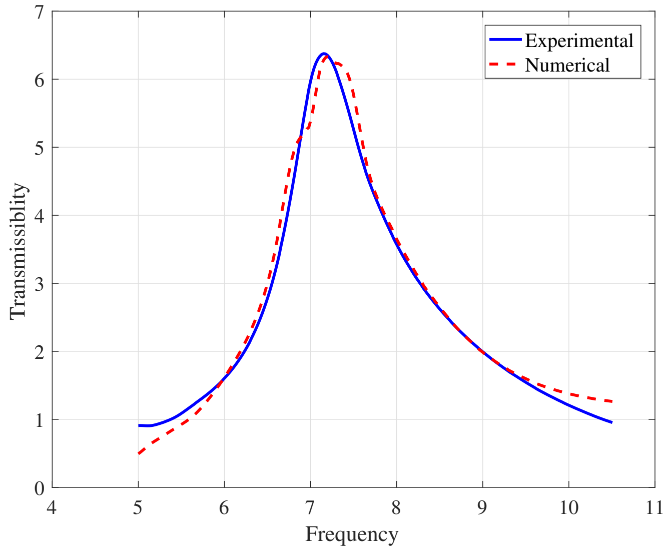

Figure 4. Comparison between experimental and numerical results of WMVD under sine-sweep excitation

Thus, the mathematical models of stiffness and damping could be written as Eqs.(6) and (7), respectively:

$$K(X) = 2.6980\,10^4 - 1.9842\,10^7\,X + 1.0963\,10^{10}\,X^2 - 3.0622\,10^{12}\,X^3 \\ +4.1697\,10^{14}\,X^4 - 2.1911,10^{16}\,X^5 \tag{6}$$

$$C(X,\dot{X}) = 345.8028 - 2.7054\,10^5\,X - 2.1222\,10^9\,X^2 + 4.6125\,10^{11}\,X^3 \\ +4.8549\,10^3\,\dot{X} - 1.0710\,10^6\,\dot{X}^2 + 9.5060\,10^7\,\dot{X}\,X \\ +2.2852\,10^8\,\dot{X}^2\,X - 2.0484\,10^{10}\,\dot{X}\,X^2 \tag{7}$$

Figure 4 depicts a comparison between the measured data and the numerical simulation of the WMV damper, where the stiffness and damping functions, defined above, are used to iteratively solve Eq. (1). It is noticed that the developed mathematical model could capture the softening characteristic (i.e. transmissibility curves are trended to the left) of the damper with good accuracy. Furthermore, the peak resonance is perfectly predicted; less than 0.56 % frequency error with superior to 0.6 % amplitude error between experimental and numerical results. Nevertheless, undesirable kinks appear for the numerical transmissibility and this slight error is explained by the limitations of the surface fitting toolbox of MATLAB. With the increase of the polynomial order, the goodness of fit increases, however, additional terms of the mathematical model increase the complexity and may cause a numerical instability. This error could not affect the predicted behavior of the nonlinear system due to the good agreement of the resonance even the width of the curve.

2.2. Matlab Simscape Multibody^{TM} model of the WMVD isolated system

Matlab Simscape Multibody^{TM} is used to simulate the WMVD isolated system by modeling through physical blocks. Figure 5(a) shows the developed multibody model of the WMVD isolated system. The different bodies, constituting the studied system, are interconnected through weld blocks that define the degrees of freedom between them. The dynamic responses are determined based on the Simscape Multibody^{TM} solver with variable time step. The displacement, velocity and acceleration responses of the system are sensed through the Transform sensor block. The mechanical configuration block defines gravity and the Word Frame block is used to define the reference frame.

Inside the anti-seismic support model (Figure 5(b)), the WMVD components are connected to two rigid body blocks representing the upper and lower plates. Here, prismatic joint blocks are used to define the vertical movements of the WMVD isolated system in space relative to the Z axis. The external force is applied to the bodies through the actuation method, where the force is provided by input and the motion is automatically computed.

The WMVD model is a collection of physical signals blocks which must be appropriately connected to simulate the dynamic system. The physical signals model that uses the mathematical model (Eqs. 6 and 7) to relate the displacement and velocity with nonlinear stiffness and damping is created in Matlab Simscape^{TM} environment. Then, the created physical model is connected to the variable translational spring/damper blocks, which represent the translational spring /viscous damper with variable stiffness/damping coefficients, as shown in Figure 5(c). These physical blocks are gathered from Physical Libraries, while physical block parameters are imported from the mathematical model parameters identified above. The stiffness/damping physical model is extended and mechanical model is developed using SimscapeMultibody^{TM} to describe the seismic isolation system behavior. To interface Simscape Multibody^{TM} components with Simscape physical blocks that model the

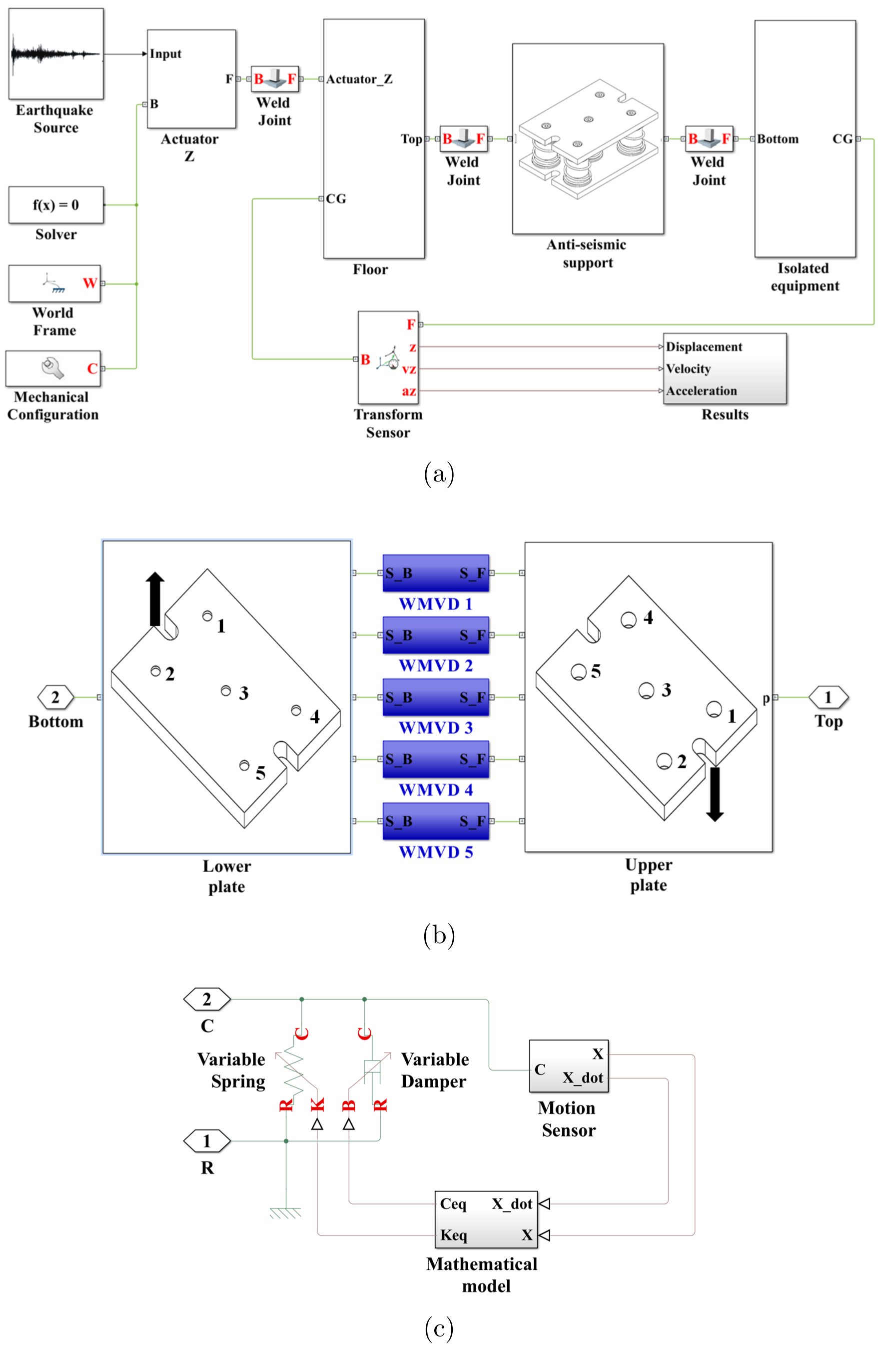

Figure 5. (a) Multibody model of WMVD isolated system, (b) Anti-seismic support with metallic dampers model and (c) Stiffness/damping model of WMVD, created via Matlab Simscape Multibody^{TM}

stiffness and damping, a Force Sensor block outputs forces signal applied to the joint blocks. The velocity of the multibody component can be constrained to the velocity of the physical component by passing a measured velocity physical signal to a Velocity Source block.

2.3. Artificial seismic time-history generation procedure

The earthquake simulation is crucial to significantly facilitate the study of structural safety against the additional cumulative damage during seismic excitation. However, the main difficulty in the earthquake ground motion modeling stems from their frequency content. In fact, the earthquake acceleration, velocity, and displacement, transmitted through the primary structure, are amplified by influencing factors (i.e. the earthquake magnitude, the distance-to-side and the building components effects). Thus, entering an actual earthquake as input for seismic analysis is not large enough to obtain sufficiently accurate results. In order to avoid the scarcity of ground motion records, an artificial seismic time-history generation procedure is used to synthesize a seismic time history based on the non-stationary features of real earthquake accelerograms, in the first concern, and compatible with the GR-63-CORE (Zone 4) response spectrum, in the second concern. The GR-63-CORE standard provides environmental design guidelines, with the highest seismic risk category (Zone 4), for IT equipment in order to "simulate conditions that would be encountered in service when building floors apply earthquake motions to the equipment" [36, 37].

2.3.1. Description of the generation procedure

As demonstrated in Figure 6, the synthetic seismic time history is firstly generated for a real earthquake. Next, the generated earthquake is scaled up or down to match with GR-63-CORE (Zone 4) response spectrum.
In the first step, the initial artificial earthquake time history is generated, to mimic the characteristics of an original earthquake. This is by using the generalization of the Kanai-Tajimi model [38–41] and the adjusted time-modulating function. The latter is required to convert a stationary Gaussian process to a non-stationary process. Stationary Gaussian white noise stochastic time series are generated using the expression according to:

$$\ddot{U}_g^{ST} = \sum_{r=1}^{N} \sqrt{4G_{\ddot{U}_g}(r\Delta\omega)}\,\cos(r\Delta\omega t + 2\pi\theta_r) \tag{8}$$

where θ_r is the random value and $\Delta\omega$ is the frequency step. $G_{\ddot{U}_g}$ is the appropriate Power Spectral Density (PSD) function defined according to Kanai–Tajimi model [38, 39]:

$$G_{\ddot{U}_g} = G_0 \frac{1 + 4\xi_g^2(\frac{\omega}{\omega_g})}{(1 - (\frac{\omega}{\omega_g})^2)^2 + 4\xi_g^2(\frac{\omega}{\omega_g})^2} \tag{9}$$

where ξ_g and ω_g represent two parameters of the original Kanai-Tajimi model; the site dominant damping coefficient and the time dependent predominant ground frequency, respectively. G_0 is the constant power spectral intensity of the bedrock excitation.

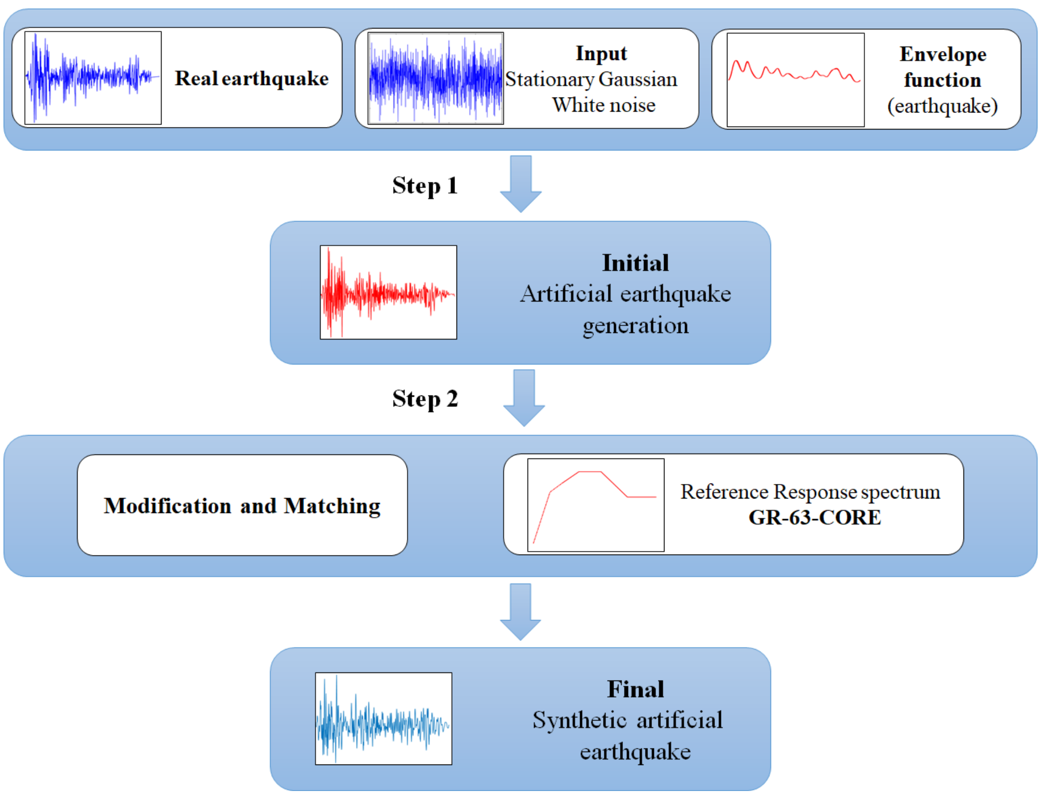

Figure 6. Flow chart of the artificial seismic time history generation procedure

The improved version of the Kanai–Tajimi model was introduced in [40, 41] to capture the nonstationary feature of the real earthquake records and given by:

$$\ddot{X}_f + 2\xi_g(t)\omega_g(t)\dot{X}_f + \omega_g^2(t)X_f = \ddot{U}_g^{ST}(t) \tag{10}$$

$$\ddot{X}_g = -(2\xi_g(t)\omega_g(t)\dot{X}_f + \omega_g^2(t)X_f)\ \mathrm{e}(t) \tag{11}$$

where $e(t)$ denotes the time-modulating function. X_f is the filter response, solved via the central difference algorithm. Substituting the displacement X_f and the velocity $\dot{X}_f$ of Eq.(10) into Eq.(11) leads to the artificially generated non-stationary earthquake.

In this study, the ξ_g is assumed to be a constant, that depends on the natural earthquake, and the acceleration record is statically analyzed to estimate ω_g and $e(t)$.

In order to estimate the time-dependent frequency ω_g, the moving-time-window procedure is used. Firstly, the time-average zero-crossing rate is evaluated:

$$\hat{F}_c(t) = \frac{Z_c|_{t=\pm\frac{t_w}{2}}}{t_w} \tag{12}$$

where Z_c denotes the number of zero axis crossing within the time interval $[-\frac{t_w}{2};\frac{t_w}{2}]$ and t_w is the time-window size. Then, Gaussian time function is fitted to the data for the zero-crossing rate and the time-dependent frequency function is now given by:

$$\omega_g = \pi\hat{F}_c(t) \tag{13}$$

where $\widehat{F}_c(t)$ is the Gaussian time function fitted for the original accelerogram. To generate an acceleration record whose time characteristics are in proper agreement with those of an original record, an optimal time-modulating function, $e(t)$, should be estimated. Zheng Li et al. [42] abandoned the deterministic function and proposed to adjust the time-modulating shape according to the quotient between the target and simulated energy distributions. The energy distributions, in the time domain, are written as:

$$I(t) = \ddot{U}_g(t)^2 \tag{14}$$

where $\ddot{U}_g$ denotes the time-history accelerogram. To avoid the problem of convergence in the determination of the energy content, an average $I_{a,i}$ is introduced instead of the original and obtained by:

$$I_a(t_i) = \frac{I(t_{i-1}) + I(t_{i+1})}{2} \tag{15}$$

Then, the shape of the time-modulating function could be updated based on the ratio between $I_{a,t\arg et}$ and $I_{a,computed}$.

$$e_{j+1}(t) = \left(\frac{I_{a,t\arg et}}{I_{a,compted}}\right)^p e_j(t) \tag{16}$$

where e_{j+1} and e_j are the envelope shapes of the j^{th} and $j+1^{th}$ iterations. $I_{a,t\arg et}$ and $I_{a,computed}$ represent the energy distributions of the original and the new time history accelerograms, respectively. p represents the specified factor to control the convergence speed.

In the second step, a scaling and matching method is iteratively applied to the initial generated time history accelerogram in order to meet the criteria required by the GR-63-CORE standard [36]. The Given Response Spectrum (GRS) shall envelop the Required Response Spectra (RRS) between 1 and 50 Hz, while, it should not exceed by more than 30 % in the frequency range of 1 to 7 Hz. The RRS is drawn at 2 % damping in the frequency range of 0.3 to 50 Hz, with a resolution of 6 division per octave.

The original motion is primarily scaled so that the Peak Ground Acceleration (PGA) matched the product of the ZPA to a predefined scale factor. In order to have a good initial approximation of the matched accelerogram, the predefined scale factor is tuned and after several numerical tests the more appropriate values are found to be about 0.8-1.

Subsequently, an iterative scheme has been considered in which the time history is modified so that the response spectrum of the new time history should satisfy the requirements, mentioned above. For each iteration, the response spectrum of the generated accelerogram is scaled up or down based on the ratio of the calculated response spectrum (CRS) to the given response spectrum (GRS) at a given octave frequency (between 0.3 and 50 Hz). The ratio between the GRS and the CRS can be denoted as follows:

$$R(\omega_n, \xi) = \frac{CRS(\omega_n, \xi)}{GRS(\omega_n, \xi)} \tag{17}$$

The Fourier transform of the new time history at step (j+1) can now be calculated by the following equation:

$$A_{n,j+1} = \frac{A_{n,j}}{R(\omega_n, \xi)} \tag{18}$$

Now, with the new magnitude for step (j+1) set to $A_{n,j+1}$, the time history for step (k+1), $\ddot{x}_{j+1}(t)$ can once again be obtained using inverse Fourier transform. After that, the new CRS can be updated, which leads to a new response spectrum ratio at step (j+1). The iterative producers continues until the relative error, β, between the response spectrum of new time history and the required response spectrum has fallen in the specified tolerance limit:

$$\beta = \frac{\|TRS - CRS\|}{\|CRS\|} \tag{19}$$

2.3.2. Application of generation procedure for natural earthquakes

The proposed procedure for the simulation of ground acceleration time histories is applied now to generate an artificial accelerogram for different natural accelerograms, satisfied the requirement prescribed by the GR-63-CORE Standard. Natural accelerograms are recorded during historical earthquakes and selected from the databases of the Strong-Motion Virtual Data Center (VDC). Earthquake records are listed in Table 1.

Table 1. Characteristics of ground motions

Earthquake	**Year**	**Station**	M_w	**PGA** (cm/s^2)	**PGV** (cm/s)	ξ_g
El Centro	1940	El Centro, CA-Array ♯ 9	6.9	341.69	33.45	0.42
Tabas	1978	Tabas, Iran	7.4	864.36	100.00	0.35
Manjil	1990	Abbar, Iran	7.4	504.61	-	0.3
Kobe	1995	Takatori, Japan	6.9	599.59	-	0.1

In this section, a constant power spectral intensity of $G_0 = 1\ cm^2/s^3$, a time interval of $\Delta T = 0.02\ s$ and a time-window size of 2 s are used for the stationary Gaussian white noise process generation [40]. The GRS is taken to be the RRS (GR-63-CORE (Zone 4)) multiplied by 1.15 to be the middle of the permissible region. Figures 7 and 8 compare the generated accelerograms with the historical earthquakes of El Centro and Kobe records, respectively. It is shown that the generated accelerograms preserve the time and frequency characteristics of the original records.
The response spectra and the scaled accelerograms are displayed in Figures 9 and 10. It is noted that the response spectra of the synthetic earthquake

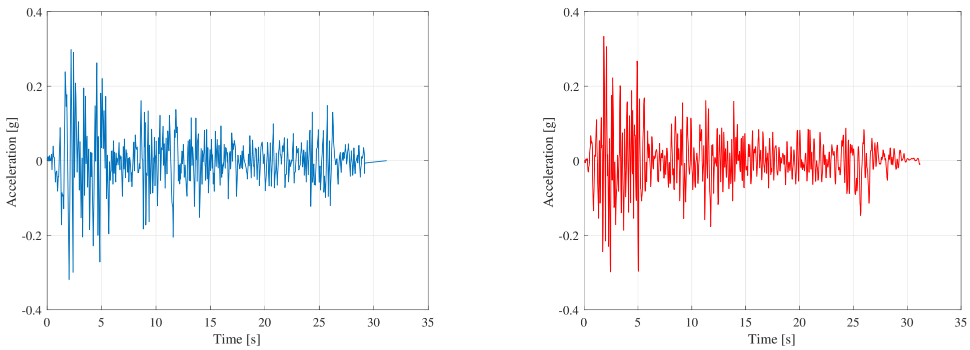

(a) (b)

Figure 7. (a) Original, (b) Generated ground motion accelerograms of El Centro record

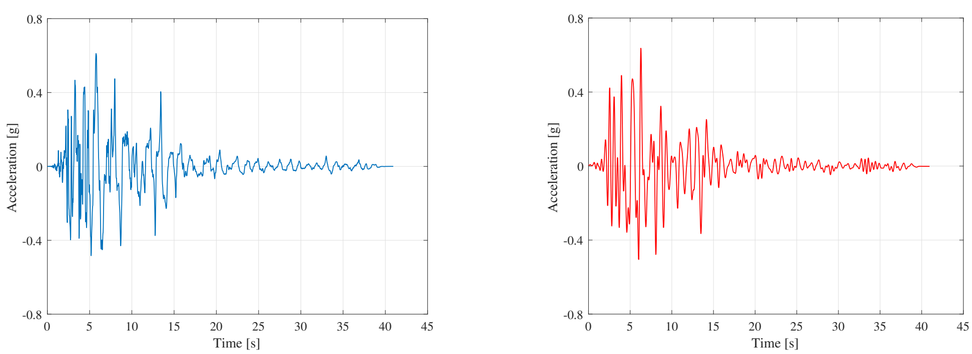

(a) (b)

Figure 8. (a) Original, (b) Generated ground motion accelerograms of KOBE record

satisfy the necessary criteria (i.e. should envelop the RRS in the range of frequencies of 1 to 50 Hz and not exceed the RRS by more than 30 % in the frequency range of 1 to 7 Hz). The scaled accelerograms still preserve the time characteristics of the original records, in addition, succeed at capturing the required acceleration content at low frequencies (i.e. higher than 0.2 g at 0.3 Hz). In fact, the building attenuates the high frequency vibrations and remains on the low frequency vibrations that are transferred to the sensitive equipment located in the floor inside the building [41]. Thus, the low frequency vibrations need more attention in the safety study of the seismic isolation system designed for protecting sensitive equipment.

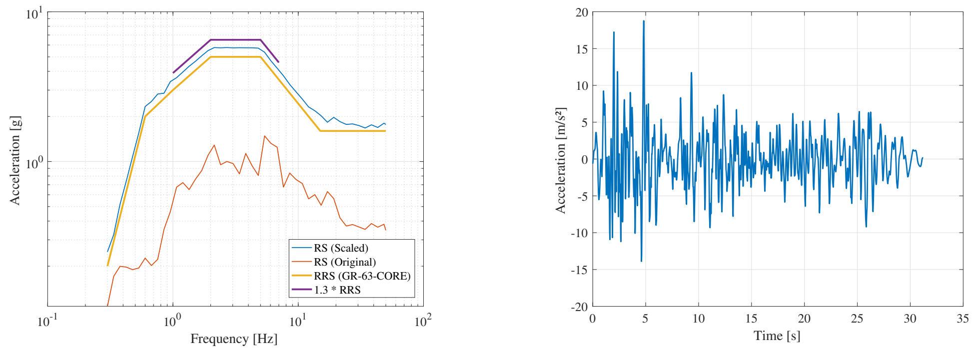

(a) (b)

Figure 9. (a) Response spectrum of artificial accelerogram scaled to 1.15 RRS, (b) Scaled time history for El Centro record

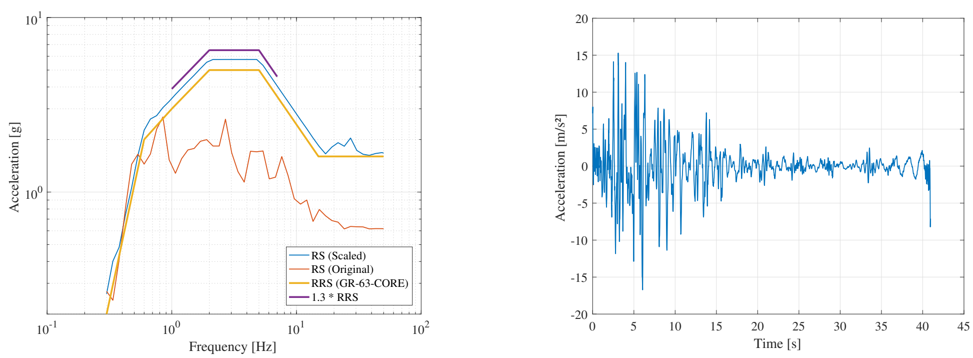

(a) (b)

Figure 10. (a) Response spectrum of artificial accelerogram scaled to 1.15 RRS, (b) Scaled time history for KOBE record

3. Dynamic analysis of wire mesh vibration damper isolated system

For the seismic isolation performance investigation purposes, the sensitive equipment mounted on the WMVD, which is considered as rigid body with mass of 30 kg (including the upper plate and the isolated equipment), is subjected to a series of artificial earthquake ground motions, generated in

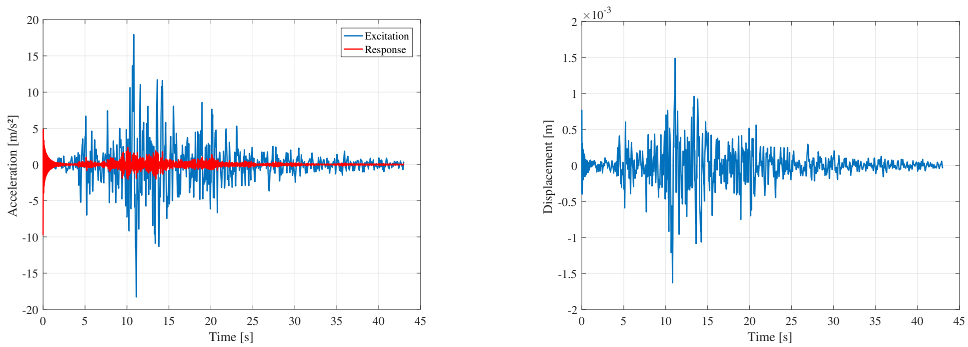

(a) (b)

Figure 11. (a) Acceleration and (b) Displacement Response of WMVD under the far-field artificial earthquake (TABAS record)

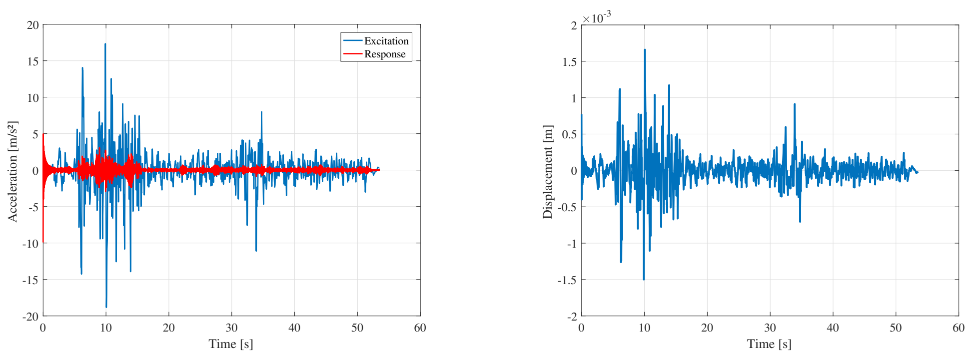

(a) (b)

Figure 12. (a) Acceleration and (b) Displacement Response of WMVD under the near-field artificial ground motion (MANJIL record)

Section 2. In detail, two acceleration records measured from historical earthquakes with different characteristics will be selected to perform the seismic analysis. The record from Tabas (Tabas-Iran station) earthquake, characterized by strong long-period waveform, is typically classified as near-fault ground motion. The record from Manjil (Abbar-Iran station) earthquake, contained fewer long-period waves components, is used to represent far-field ground motion. Since the isolated equipment is assumed to behave as a rigid body, the response of the WMVD is equivalent to the response of the whole WMVD isolated system.

Figures 11(a) and 12(a) depict the acceleration response time histories of the WMVD, when the isolated equipment is subjected to the near-field earthquake record (Tabas) and far-field earthquake record (Manjil), respectively. Figures 11(b) and 12(b) display the displacement response time histories relative to the moving floor-ground, with respect to the static equilibrium position of the mass under gravity when the base is fixed. It is observed that the WMVD has very good performance in the Tabas and Manjil earthquakes since it is able to reduce the transmitted ground motion acceleration from $18\,m/s^2$ to less than $2.5\,m/s^2$ and from about $19\,m/s^2$ down to $3\,m/s^2$, respectively.

In order to investigate the isolation efficiency of the WMVD under artificial earthquake ground motions, the results are compared with seismic responses obtained considering the sensitive equipment linearly isolated. To this aim a comparative analysis, based on the geometric criterion, is adopted to assess the nonlinear behavior of the WMVD in the seismic mitigation. The linear anti-seismic support, commercially used for the vibration isolation applications, is composed of five linear coil springs with similar geometric properties as the WMVD. In fact, the achievement of the best performance of the linear seismic isolation system would require higher stiffness and damping. However, it is well-known that higher values of stiffness and damping generally lead to large size of the linear isolator (i.e. mean diameter, free length, wire diameter, ...). Therefore, this aspect is discrepancy with the comparative analysis criterion (i.e. the use of two kinds of isolation devises with the same geometric conditions). The Stiffness/damping model of the linear isolator is determined throughout the identification methodology, given in Section 2. Table 2 illustrates the linear isolator parameters.

Table 2. The Stiffness/damping model of the linear isolator

	Mathematical Model	**Coefficients**	**Basic Functions**
Stiffness	$P_{00}^{stiff} B_{00}^{stiff}(X, \dot{X})$ (Eq.(2))	$1.26\,10^4$ $[N/m]$	$\{1\}$ (Eq.(4))
Damping	$P_{00}^{damp} B_{00}^{damp}(X, \dot{X})$ (Eq.(3))	11.877 $[Ns/m]$	$\{1\}$ (Eq.(5))

From Figure 13, it is evident that in both earthquakes, the proposed WMVD is very effective in the seismic mitigation of the system acceleration, as compared to the linearly isolated system. The acceleration responses of the linear system increased by more than 160 % as compared to the ground motion acceleration. Moreover, in the comparison of near and far-field effects on the WMVD performance, the maximum acceleration and displacement responses are plotted in Figure 14. It is noticed that, as mentioned above, the mitigation in the transmitted ground acceleration is equivalent to 85 % reduction when the system is subjected to the near and far-field earthquakes. This implies that the WMVD is suitable for both kinds of earthquakes.

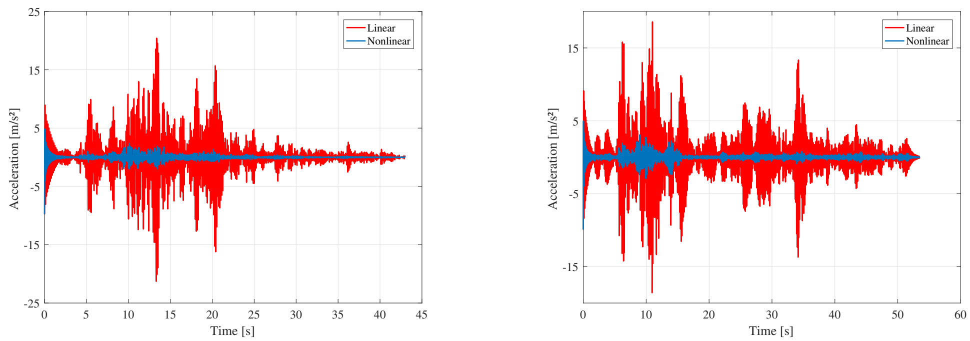

(a) (b)

Figure 13. Comparative analysis: Acceleration responses of linearly and WMVD isolated systems subjected to: (a) TABAS and (b) MANJIL records

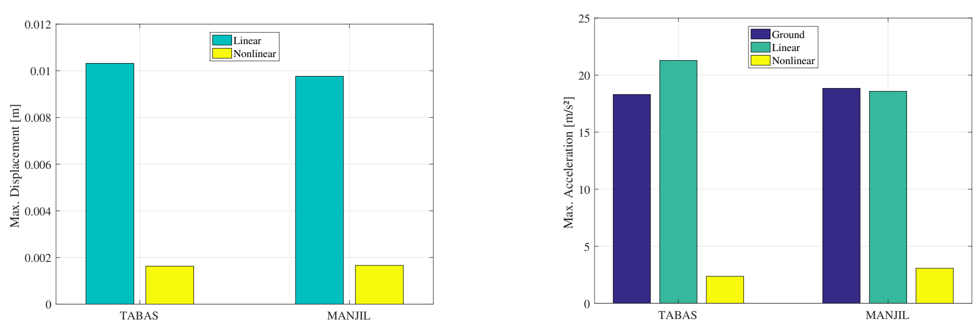

(a) (b)

Figure 14. Peak responses of linearly and WMVD isolated systems: (a) Displacement, (b) Acceleration

4. Seismic probabilistic risk assessment

The development of fragility curves, which is a widely used approach for the seismic probabilistic risk assessment, attempts to estimate the probability of exceeding a certain threshold for vibration-sensitive equipment subjected to specific seismic excitation level. The fragility curves are generated by first determining the demand parameters from Incremental Dynamic Analysis.

4.1. Incremental dynamic analysis

Incremental Dynamic Analysis (IDA) is a parametric analysis technique, which is implemented to assess the seismic performance of the studied isolation system under artificial earthquakes. Several suites of accelerograms with different GRS profiles (i.e. different RRS multipliers) are used to develop simplified fragility curves in terms of the maximum acceleration. A range of intensities is assessed by varying RRS multipliers between 0.5 and 1.5, with an increment step of 0.05. Each suite of 50 earthquake ground motions is simulated using the artificial seismic time-history generation procedure, described in Section 2, and then scaled. The scaling factor is equivalent to median value of the peak ground acceleration of the 50 artificial accelerograms compatible with the selected GRS (corresponding to RRS multiplier).

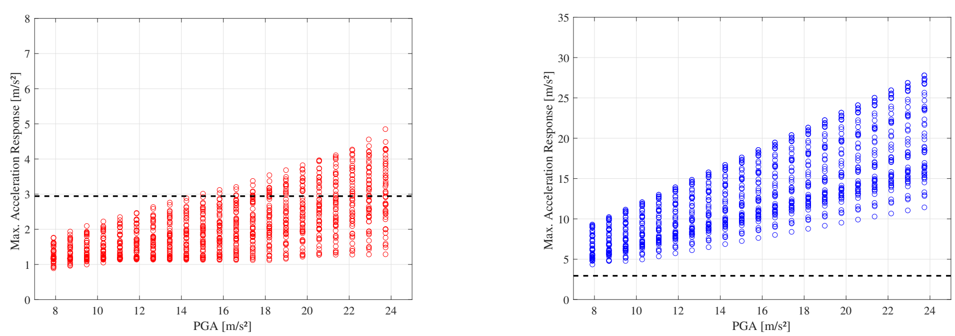

(a) (b)

Figure 15. Result of the Incremental Dynamic Analysis for: (a) WMVD and (b)linearly isolated systems under artificial accelerograms (TABAS earthquake)

IBM [43] defined the Vibration-sensitive equipment performance with a single limit state related to the maximum acceleration responses (MAR) of the isolated components. Therefore, the parameter linked to the failure modes is quantified through the probability that the MAR exceeds a tolerable limit. Accordingly, in order to avoid damage and loss of the functionality, POWER7 information [43] supplied tolerable limits, varied 0.1 g and 0.8 g peak acceleration depending on the vibration environment. In practice, the allowable limit on acceleration response, is assumed to be 0.3 g ($\sim 3\,m/s^2$) [44]. The maximum responses distribution of MWVD and linearly isolated systems are plotted in the stripe form corresponding to each PGA level, as shown in Figures 15(a) and 15(b), respectively.

4.2. Fragility analysis

The fragility curves or functions that represent the probability of exceeding a given limit state under a set of the accelerograms, are derived by determining the probabilistic seismic demand model (PSDM). Generally, the PSDM provides a relation between an Engineering Demand Parameter (EDP) and an Intensity Measure (IM), expressed as:

$$EDP = a(IM)^b \tag{20}$$

In the PSDM approach, a logarithmic correlation between the selected EDP and the IM is defined as shown below:

$$\ln(EDP) = \ln(a) + b\ln(IM) \tag{21}$$

here a and b are constants and the response data obtained from IDA are used to estimate unknown coefficients through a linear regression analysis. The dispersion accounting for the uncertainty in the relation, denoted as $\beta_{EDP/IM}$ and conditioned upon the IM, is calculated using Eq.(22):

$$\beta_{EDP/IM} = \sqrt{\frac{\sum_{i=1}^{N} \left(\ln(EDP_i) - \ln a(IM)^b\right)^2}{N-2}} \tag{22}$$

where N is the number of simulations and EDP_i and $a(IM)^b$ represent the calculated demand parameter from the IDA and the PSD model, respectively. With the established probabilistic seismic demand models and the defined limit state, it is now possible to generate fragility functions, corresponding to cumulative probability of exceeding a certain limit state for given IM, using

Eq.(23):

$$P\left[LS/IM\right] = \Phi\left[\frac{\ln(IM) - \ln(\mu)}{\beta_{comp}}\right] \tag{23}$$

$\Phi\left[.\right]$ is the standard cumulative distribution function and μ represents the median value of IM for considered limit state, expressed as:

$$\ln(\mu) = \frac{\ln(S_c) - \ln(a)}{b} \tag{24}$$

β_{comp} denotes the dispersion component and presented in:

$$\beta_{comp} = \sqrt{\frac{\beta^2_{EDP/IM} + \beta^2_c}{b}} \tag{25}$$

where S_c and β_c are the median and the dispersion values for the system limit state, respectively.

In this study, the ground motion, PGA, and the maximum acceleration response (MAR) are chosen as the intensity measure (IM) and the engineering demand parameter (EDP), respectively. The isolated equipment loses their functionality when the MAR exceeds a certain threshold:

$$a_{\max} \geq c \tag{26}$$

where c is the allowable limit on acceleration response, taken to be 0.3 g, which if exceeded constitutes a failure of the isolation system to perform adequately.

The response data of the MWVD under artificial accelerograms (TABAS earthquake), generated by IDA, were used to create the Probabilistic Seismic Demand Models (PSDMs). Figure 16(a) represents the PSDMs of MAR as function of the PGA of the scaled accelerogram by varying RRS multipliers between 0.5 and 1.5. The corresponding linear regression equation of the PSDMs for the maximum acceleration response is given as:

$$\ln(MAR) = \ln(0.2169) + 0.7971\ \ln(PGA) \tag{27}$$

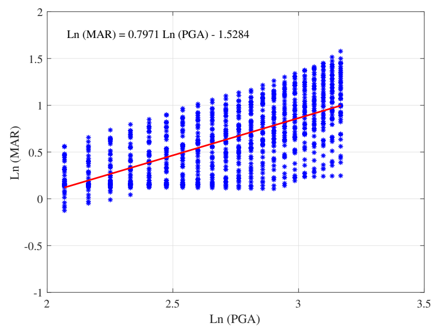

(a)

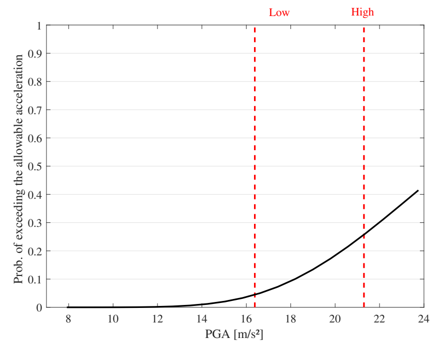

(b)

Figure 16. (a) PSDM and (b) fragility curves of maximum acceleration response for artificial accelerograms (TABAS earthquake)

From Eq.(23), it is evidently noted that the necessary parameters to describe the cumulative distribution are the logarithmic median μ and the dispersion component β_{comp}, which is calculated using the linear regression analysis of ln(MAR) on ln(PGA) (Eq.(22)). The median is then calculated from Eq.(24) corresponding to the aforementioned threshold value.
Figure 16(b) shows the fragility curves constructed by plotting the probability of exceeding a given allowable acceleration as the PGA of generated and scaled accelerograms. The black curve is associated with the allowable acceleration of 0.3 g (representing the limit capacity of the considered WMVD). The red dashed lines represent the region associated with the records that satisfy the GR-63-CORE requirements. It can be observed that the probability of exceeding the sensitive components tolerable limit for the isolated equipment mounted on the WMVD is of the order of about 5 % at low PGA level and below 30 % at high PGA level. Results clearly indicate the benefit of using WMVD for reducing the seismic motion transmitted to the vibration-sensitive equipment and avoid the risk of loss the functionality.

Conclusion

For the protection of vibration-sensitive equipment, such as IT equipment, from horst floor motions, a passive isolator, called Wire Mesh Vibration Damper (WMVD) is proposed and investigated in this study. The WMVD is given as combination of linear coil-spring and nonlinear metallic cushion damper.

As a first step in the seismic isolation effectiveness study, the multibody model of the WMVD isolated system is developed using Matlab Simscape Multibody^{TM}, where the mathematical model of the WMVD is defined and experimentally validated using a nonparametric identification method. In the second step, an artificial seismic time-history generation procedure is proposed to simulate several suites of generated time history accelerograms, able to simultaneously capture the time characteristics of natural earthquake records and satisfy the GR-63-CORE (Zone 4) requirements. The response spectrum of the generated earthquake should envelop the required response spectrum (RRS) prescribed by the standard between 1 Hz and 50 Hz and not exceed more than 30 % between 1 and 7 Hz.

In order to demonstrate the isolation performance of the WMVD, the defined model is implemented to analyze the seismic responses of sensitive equipment under two artificial generated and scaled accelerograms with different characteristics (near- and far-fields). The results show that the transmitted accelerations reduction is equivalent to 85 % as compared to the generated ground motions for near-field earthquake even for the far-field one. The seismic responses of the WMVD isolated system are then compared with linearly isolated system responses. The results show an increase by more than 160 % of the motion transmitted to the linearly isolated equipment, thus proving the isolation performance of the MWVD. This efficiency in mitigating the seismic response compared to the linear isolator is due to the nonlinear behavior of the metallic cushion metallic. The nonlinearity influence on the feasibility of the WMVD is manifested in the effect of high damping capacity on the seismic response amplitude reduction. Other factor includes the soft nonlinear characteristic that design a system with a high static stiffness to benefit a small static deflection, and a low natural frequency to widen the frequency region of isolation. In fact, a linear isolator is only feasible solution if the natural frequency is well below the excitation frequency. However, under long-period components disturbances, this isolator causes excessive deflection and even damage of the isolated system.

This study also presented the seismic probabilistic risk assessment of the WMVD designed for protecting sensitive equipment subjected to earthquake. Incremental Dynamic Analysis is firstly conducted to generate the data set of seismic responses considering the maximum acceleration responses as engineering demand parameter. The performance is eventually assessed by calculating the probability of exceeding the tolerable maximum acceleration of the isolated equipment as a function of peak ground acceleration levels.

The results demonstrated the benefits offered by the seismic protective system to assess the safety of the IT equipment. Low probabilities of failure (less than 30 %) can be achieved when the equipment subjected to earthquakes within the response spectra range, higher than the GR-63-CORE (Zone 4) RRS and lower than 30 % limit.

Acknowledgments

The authors acknowledges the support of "Augusto González de Linares" Post-Doctoral Fellowship POS-UC-2019-10. This work has been performed under the Project PID2020-116572RA-I00, funded by the Spanish Ministry of Science and Innovation. This support is gratefully appreciated.

References

[1] O. E. Ozbulut, S. Hurlebaus, Re-centering variable friction device for vibration control of structures subjected to near-field earthquakes, Mechanical Systems and Signal Processing 25 (8) (2011) 2849–2862.

[2] D. Cancellara, F. De Angelis, Assessment and dynamic nonlinear analysis of different base isolation systems for a multi-storey rc building irregular in plan, Computers & Structures 180 (2017) 74–88.

[3] J. Yang, S. Sun, T. Tian, W. Li, H. Du, G. Alici, M. Nakano, Development of a novel multi-layer mre isolator for suppression of building vibrations under seismic events, Mechanical systems and signal processing 70 (2016) 811–820.

[4] E. García-Macías, F. Ubertini, Seismic interferometry for earthquake-induced damage identification in historic masonry towers, Mechanical Systems and Signal Processing 132 (2019) 380–404.

[5] Y. Lei, J. Lu, J. Huang, S. Chen, A general synthesis of identification and vibration control of building structures under unknown excitations, Mechanical Systems and Signal Processing 143 (2020) 106803.

[6] F. Hedayati-Dezfuli, M. S. Alam, Seismic vulnerability assessment of a multi-span continuous steel-girder bridge isolated by sma wire-based natural rubber bearings (sma-nrb), in: Structures Congress 2015, 2015, pp. 597–606.

[7] A. Billah, M. Alam, Performance based seismic design of concrete bridge pier reinforced with shape memory alloy-part 1: Development of performance-based damage states, ASCE J. Struct. Eng 142 (12) (2016) 1–11.

[8] N. Xiang, X. Chen, M. S. Alam, Probabilistic seismic fragility and loss analysis of concrete bridge piers with superelastic shape memory alloy-steel coupled reinforcing bars, Engineering Structures 207 (2020) 110229.

[9] S. Kitayama, D. Lee, M. C. Constantinou, L. Kempner Jr, Probabilistic seismic assessment of seismically isolated electrical transformers considering vertical isolation and vertical ground motion, Engineering Structures 152 (2017) 888–900.

[10] D. Wang, Y. Zhang, C. Wu, G. Xue, W. Huang, Seismic performance of base-isolated ap1000 shield building with consideration of fluid-structure interaction, Nuclear Engineering and Design 353 (2019) 110241.

[11] G. Jia, I. Gidaris, A. A. Taflanidis, G. P. Mavroeidis, Reliability-based assessment/design of floor isolation systems, Engineering structures 78 (2014) 41–56.

[12] S. Liu, G. P. Warn, Seismic performance and sensitivity of floor isolation systems in steel plate shear wall structures, Engineering structures 42 (2012) 115–126.

[13] C. Alhan, F. Şahin, Protecting vibration-sensitive contents: an investigation of floor accelerations in seismically isolated buildings, Bulletin of Earthquake Engineering 9 (4) (2011) 1203–1226.

[14] M. Hamidi, M. El Naggar, On the performance of scf in seismic isolation of the interior equipment of buildings, Earthquake engineering & structural dynamics 36 (11) (2007) 1581–1604.

[15] P. S. Harvey Jr, H. P. Gavin, Assessment of a rolling isolation system using reduced order structural models, Engineering Structures 99 (2015) 708–725.

[16] M. Ismail, J. Rodellar, F. Ikhouane, An innovative isolation bearing for motion-sensitive equipment, Journal of Sound and Vibration 326 (3-5) (2009) 503–521.

[17] R. Ibrahim, Recent advances in nonlinear passive vibration isolators, Journal of sound and vibration 314 (3-5) (2008) 371–452.

[18] M. D. Symans, M. C. Constantinou, Semi-active control systems for seismic protection of structures: a state-of-the-art review, Engineering structures 21 (6) (1999) 469–487.

[19] T. M. Al-Hussaini, M. C. Constantinou, V. A. Zayas, Seismic isolation of multi-story frame structures using spherical sliding isolation systems, National Center for earthquake engineering research, 1994.

[20] P. S. Harvey Jr, K. C. Kelly, A review of rolling-type seismic isolation: Historical development and future directions, Engineering Structures 125 (2016) 521–531.

[21] P. S. Harvey Jr, H. P. Gavin, Double rolling isolation systems: a mathematical model and experimental validation, International Journal of Non-Linear Mechanics 61 (2014) 80–92.

[22] H. P. Gavin, A. Zaicenco, Performance and reliability of semi-active equipment isolation, Journal of Sound and Vibration 306 (1-2) (2007) 74–90.

[23] C. Alhan, H. P. Gavin, Reliability of base isolation for the protection of critical equipment from earthquake hazards, Engineering Structures 27 (9) (2005) 1435–1449.

[24] V. Lambrou, M. C. Constantinou, Study of seismic isolation systems for computer floors, National Center for Earthquake Engineering Research, 1994.

[25] P. Murnal, R. Sinha, Aseismic design of structure–equipment systems using variable frequency pendulum isolator, Nuclear Engineering and Design 231 (2) (2004) 129–139.

[26] L.-Y. Lu, C.-C. Lin, G.-L. Lin, C.-Y. Lin, Experiment and analysis of a fuzzy-controlled piezoelectric seismic isolation system, Journal of Sound and Vibration 329 (11) (2010) 1992–2014.

[27] P. Xiang, A. Nishitani, Seismic vibration control of building structures with multiple tuned mass damper floors integrated, Earthquake Engineering & Structural Dynamics 43 (6) (2014) 909–925.

[28] A. Javanmardi, Z. Ibrahim, K. Ghaedi, H. B. Ghadim, M. U. Hanif, State-of-the-art review of metallic dampers: Testing, development and implementation, Archives of Computational Methods in Engineering 27 (2) (2020) 455–478.

[29] F. Paolacci, R. Giannini, Study of the effectiveness of steel cable dampers for the seismic protection of electrical equipment, in: Proceedings of 14th World Conference on Earthquake Engineering, 2008, pp. 12–17.

[30] G. Di Massa, S. Pagano, E. Rocca, S. Strano, Sensitive equipments on wrs-btu isolators, Meccanica 48 (7) (2013) 1777–1790.

[31] S. Alessandri, R. Giannini, F. Paolacci, M. Malena, Seismic retrofitting of an hv circuit breaker using base isolation with wire ropes. part 1: Preliminary tests and analyses, Engineering Structures 98 (2015) 251–262.

[32] B. Zhang, Z. Lang, S. Billings, G. Tomlinson, J. Rongong, System identification methods for metal rubber devices, Mechanical systems and signal processing 39 (1-2) (2013) 207–226.

[33] D. Sciulli, Dynamics and control for vibration isolation design, Ph.D. thesis, Virginia Tech (1997).

[34] F. Mezghani, A. F. del Rincón, M. A. B. Souf, P. G. Fernandez, F. Chaari, F. V. Rueda, M. Haddar, Alternating frequency time domains identification technique: Parameters determination for nonlinear system from measured transmissibility data, European Journal of Mechanics-A/Solids 80 (2020) 103886.

[35] S. VIRLAB, Standard Test Procedure for the Seismic Qualification of Electrical Cabinets according to GR63-CORE (ZONE 4), issue 4 (dated 20/02/2018).

[36] T. Technologies, Nebs requirements: Physical protection, GR-63-CORE (2006).

[37] M. H. Tehrani, P. S. Harvey, Generation of synthetic accelerograms for telecommunications equipment: fragility assessment of a rolling isolation system, Bulletin of Earthquake Engineering 17 (3) (2019) 1715–1737.

[38] K. Kanai, Semi-empirical formula for the seismic characteristics of the ground, Bulletin of the Earthquake Research Institute, University of Tokyo 35 (2) (1957) 309–325.

[39] H. Tajimi, A statistical method of determining the maximum response of a building during earthquake, PROCEEDING OF WORLD CONFERENCE ON EARTHQUAKE ENGINEERING, 1960.

[40] F. Fan, G. Ahmadi, Nonstationary kanai-tajimi models for el centro 1940 and mexico city 1985 earthquakes, Probabilistic Engineering Mechanics 5 (4) (1990) 171–181.

[41] F. Rofooei, A. Mobarake, G. Ahmadi, Generation of artificial earthquake records with a nonstationary kanai–tajimi model, Engineering Structures 23 (7) (2001) 827–837.

[42] Z. Li, P. Kotronis, H. Wu, Simplified approaches for arias intensity correction of synthetic accelerograms, Bulletin of Earthquake Engineering 15 (10) (2017) 4067–4087.

[43] IBM, Power7 information: vibration and shock. systems hardware information, accessed November 2020 (updated: April 2014).

[44] C. Casey, P. Harvey Jr, W. Song, Multi-unit rolling isolation system arrays: Analytical model and sensitivity analysis, Engineering Structures 173 (2018) 656–668.